Electrochimica Acta 370 (2021) 137723

Contents lists available at ScienceDirect

Electrochimica Acta

journal homepage: www.elsevier.com/locate/electacta

One-step synthesis of γ-Fe_2O_3/Fe_3O_4 nanocomposite for sensitive electrochemical detection of hydrogen peroxide

Tatyana Molodtsova[a,*], Mikhail Gorshenkov[b], Alexey Saliev[a], Vladislav Vanyushin[b], Igor Goncharov[c], Nina Smirnova[a]

[a] Platov South-Russian State Polytechnic University (NPI), Novocherkassk 346428, Russian Federation
[b] National University of Science and Technology "MISiS", Moscow 119049, Russian Federation
[c] Belgorod National Research University, Belgorod 308015, Russian Federation

ARTICLE INFO

Article history:
Received 30 October 2020
Revised 18 December 2020
Accepted 2 January 2021
Available online 6 January 2021

Keywords:
γ-Fe_2O_3
Fe_3O_4
Pulse alternating current
Electrochemical synthesis
H_2O_2 sensing

ABSTRACT

Maghemite/magnetite nanocomposite (γ-Fe_2O_3/Fe_3O_4) was prepared via an electrochemical method using pulse alternating current and applied for electrocatalytic reduction and sensing of hydrogen peroxide. The structural and compositional analysis of the γ-Fe_2O_3/Fe_3O_4 was characterized by XRD, SEM, TEM and XPS. Its thermal decomposition behavior was studied using TG/DSC. The mechanism for γ-Fe_2O_3/Fe_3O_4 nanocomposite formation was proposed. Furthermore, the H_2O_2 sensing performance of the γ-Fe_2O_3/Fe_3O_4 nanocomposite was evaluated in 0.1 M KH_2PO_4. The sensor exhibited a fast electron transfer process in γ-Fe_2O_3/Fe_3O_4 nanocomposite. The optimized H_2O_2 sensor revealed a remarkable low limit of detection of 0.05 μM, a wide linear range from 0.0002 to 8 mM, and a fast response time of 2 s. These results demonstrated that γ-Fe_2O_3/Fe_3O_4 prepared via an electrochemical method using pulse alternating current is a promising efficient material for electrochemical sensing of H_2O_2.

1. Introduction

Hydrogen peroxide (H_2O_2) is a simple compound, but it plays an important role in biological, environmental, pharmaceutical and others applications [1–3]. Besides its well-known cytotoxic effects hydrogen peroxide is formed in the human body as a by-product of some oxidative metabolic reactions [4,5]. Excessive amount of H_2O_2 can trigger cell proliferation that may culminate into various diseases such as cancer, cardiovascular and neurodegenerative disorders [6]. Thus the H_2O_2 detection with a reliable, rapid and economic method is of great important in many industrial fields.

A wide range of techniques including spectrophotometry [7], fluorimetry [8], and chemiluminescence [9] has been developed to detect H_2O_2. However, these methods have significant drawbacks [10]. Since H_2O_2 is an electroactive molecule, an electrochemical approach can be extensively employed for hydrogen peroxide determination [11]. The electrochemical sensing technologies have recently attracted a great deal of interest due to their simplicity, low cost, high sensitivity, and fast response [12,13].

Various materials such as noble metals and transition metal oxides [1,14,15] have been exploited as the electrocatalysts for hydrogen peroxide sensing. Magnetite (Fe_3O_4) is considered to be a suitable candidate for electrochemical sensor applications owing to its unique peroxidase-like activity, excellent biocompatibility, low toxicity, good stability and high electrochemical activity [16–20]. Moreover, maghemite, γ-Fe_2O_3, (magnetic modification of iron oxide) has been explored as an active and stable electrocatalyst for H_2O_2 reduction [21].

Many ways to prepare Fe_3O_4 and γ-Fe_2O_3 nanoparticles such as co-precipitation, microemulsion, arc-discharge, solvothermal, sonochemical, microwave-assisted, chemical vapor deposition, combustion, laser ablation, carbon arc, laser pyrolysis, sol-gel and high temperature decomposition of organic precursors have been reported [22,23]. Recently, electrochemical synthesis of magnetite and maghemite nanoparticles has gained greater attention due to its advantages over other methods including simplicity, shape and size control, and low cost [17,24–26].

In this study, the γ-Fe_2O_3/Fe_3O_4 nanocomposite was prepared via an electrochemical method using pulse alternating current (PAC). The synthesis of other metal oxide-based materials such as SnO_2-SnO, TiO_2, CuO_x, Co_3O_4/CoOOH and NiO/C nanocomposite using PAC technique has already been described in our previous reports [27–31].

The obtained γ-Fe_2O_3/Fe_3O_4 nanocomposite exhibits excellent electrocatalytic activity for H_2O_2 reduction with a wide linear range from 0.0002 to 8 mM, a low detection limit (LOD) of

* Corresponding author.
E-mail address: molodtsovatat@yandex.ru (T. Molodtsova).

https://doi.org/10.1016/j.electacta.2021.137723
0013-4686/

0.05 μM, a fast response time of 2 s, good stability and selectivity.

2. Experimental

2.1. Materials and reagents

Iron foil (99%), sodium hydroxide, hydrogen peroxide, potassium dihydrogen phosphate, potassium hydroxide, isopropyl alcohol, Nafion aqueous dispersion, bidistilled water. The nitrogen used in this study was obtained from a local supplier with a purity of 99.9999%.

2.2. One-step synthesis of γ-Fe_2O_3/Fe_3O_4 nanocomposite using PAC

The selection of appropriate synthesis conditions was made during the preliminary investigation on the influence of electrolyte nature and current density on the rate of iron oxidation and the composition of the final products.

The iron foils with the area of 1 cm^2 and thickness of 0.5 mm have been employed as the anode and cathode for the γ-Fe_2O_3/Fe_3O_4 nanocomposite preparation. Preliminary the iron electrode surfaces were mechanically polished using sandpaper and washing with bidistilled water. The electrochemical synthesis was carried out using a home designed PAC source (average current density j_a:j_c= 3:3 A/cm^2) under constant stirring at 200 rpm and cooling conditions to maintain the temperature of 50–60 °C. The electrode potentials were measured relative to an Ag/AgCl reference electrode. The aqueous solution of 2 M NaOH was used as an electrolyte. The resulting precipitate was separated by filtration using a glass filter, washed with bidistilled water to a neutral pH and dried at room temperature.

2.3. Fabrication of sensor

A typical suspension of γ-Fe_2O_3/Fe_3O_4 was prepared by dispersing γ-Fe_2O_3/Fe_3O_4 nanocomposite (7 mg) in 10% Nafion solution (10 μL) and isopropyl alcohol (1 mL) and sonicated for 30 min. 8 μL of this suspension was transferred on to the surface of the polished glassy carbon rotating disk electrode and dried at room temperature.

2.4. Characterization of γ-Fe_2O_3/Fe_3O_4 nanocomposite

The X-ray diffraction (XRD) measurements were carried out on a X-ray powder diffractometer (ARL X'TRA Thermo Fisher Scientific) using Cu Kα radiation (λ=1.5406 Å). The morphology and surface elemental composition were determined using a SEM (Tescan Vega 3 sb) equipped with an Energy Dispersive Spectrometer (EDS, Oxford Instruments x-act). TEM images were obtained using a JEOL JEM 1400 with an accelerating voltage of 120 kV. Thermal properties were studied by a differential scanning calorimetry (DSC) using SDT Q600 V20.9 Build 20 model. The measurements were carried out at a heating rate of 10 °C min^{-1} in an air atmosphere within a temperature range of 25–900 °C. X-ray photoelectron spectroscopy (XPS) were obtained with a Thermo Scientific ESCALAB 250 Xi with an Al Kα source (1486.6 eV).

A potentiostat-galvanostat (P-45X, Elins) was used to control the applied potential in a three-electrode configuration for all the cyclic voltammetry (CV) and steady-state amperometric measurements. Electrochemical impedance specta (EIS) were recorded with the frequency ranging from 1 Hz to 120 kHz. Modulated speed rotator (model AFMSRCE, PINE) was used for all the electrochemical experiments. This system contains a glassy carbon rotating disk electrode (5.0 mm diameter, PINE) with a motor controlled rotor (AFMSRX, PINE), an Ag/AgCl reference electrode (3 M KCl), and a platinum wire (99.95% purity) counter electrode. All electrochemical experiments were carried out at room temperature. All solutions were deaerated using nitrogen for at least 30 min in order to remove the dissolved oxygen.

The pH measurements were performed with a pH meter (Mettler-Toledo AG, CH).

The electrochemical surface area (ECSA) can be estimate according to the equation: ECSA = $R_f \times S$, where R_f is the roughness factor and S was usually corresponding to their geometric area (S = 0,248 cm^2, in this work). According to the double-layer capacitance (C_{dl}) of a smooth oxide surface per square centimeter (60 μF cm^{-2}) [32,33], R_f was calculated using the equation: $R_f = C_{dl}$ /60 μF cm^{-2}. The double-layer capacitance was determined via plotting the ΔI (I_a–I_c) against the scan rate of CVs, where I_a is the double-layer anodic current, I_c is the double-layer cathodic current from CV in a narrow potential window.

3. Results and discussion

3.1. Material characterization

The crystal structure and crystallinity of γ-Fe_2O_3/Fe_3O_4 nanocomposite were determined by XRD. Maghemite/magnetite crystalline peaks were observed (Fig. 1a) at 18.3°, 30.10°, 35.50°, 43.16°, 53.62°, 57.05°, 62.61°,74,03° and 86.97° assigned to the (111), (220), (311), (400), (422), (511), (440), (533), and (642) planes, respectively. All the main peaks can be indexed as both maghemite (γ-Fe_2O_3) and cubic Fe_3O_4 (space group: Fd-3 m) which are in good agreement with the reported data (ICSD № 159,971). No characteristic peaks of other impurity phases have been detected indicating high purity of the obtained product. More specifically, the crystallite size calculated using the Scherrer formula was about 30 nm.

TG results demonstrate a slight weight loss about 4% for γ-Fe_2O_3/Fe_3O_4 nanocomposite at the temperatures ranging from 25 °C to 150 °C and from 250 °C to 350 °C, and DSC results show a weak endothermic peaks at approximately 100 °C and 330 °C due to desorption of physically and chemically adsorbed water, respectively [23,34] (Fig. S1). The oxidation of magnetite to hematite occurs at temperature close to 350 °C [35] through the formation of intermediate product such as metastable maghemite [36]. No weight loss is observed for the maghemite-hematite (α-Fe_2O_3) transformation.

The morphology of the γ-Fe_2O_3/Fe_3O_4 nanocomposite was evaluated by SEM. According to the previous studies reported in the literature, it is difficult to distinguish between magnetite and maghemite due to their similar structural and magnetic properties [37]. Fig. 1b depicts SEM micrograph which reveals the two types of morphology: plate-shaped and complex (sometimes splinter). The average particle size (complex shape) is about 100 nm. The particle agglomeration was observed and the size of particle aggregates varies from 1 to 9 μm. This agglomerate formation indicates that the surface energy of the γ-Fe_2O_3/Fe_3O_4 nanocomposite is relatively strong [38,39].

The elemental map acquired by EDS is shown in Fig. S2. This analysis clearly demonstrates a uniform distribution of Fe and O elements in the structure of γ-Fe_2O_3/Fe_3O_4 nanocomposite.

The morphological properties of the γ-Fe_2O_3/Fe_3O_4 nanocomposite were determined using TEM and revealed an octahedral shape of magnetite particles, which is the main phase of the nanocomposite (Fig. 1c). The strong diffraction rings are visible in the selected area of the electron diffraction pattern (SAED) (Fig. S3) indicating the crystalline nature of the prepared magnetite product. These results were consistent with those obtained from XRD measurements. A poorly crystallized maghemite was formed because of the application of low-temperature synthesis [40].

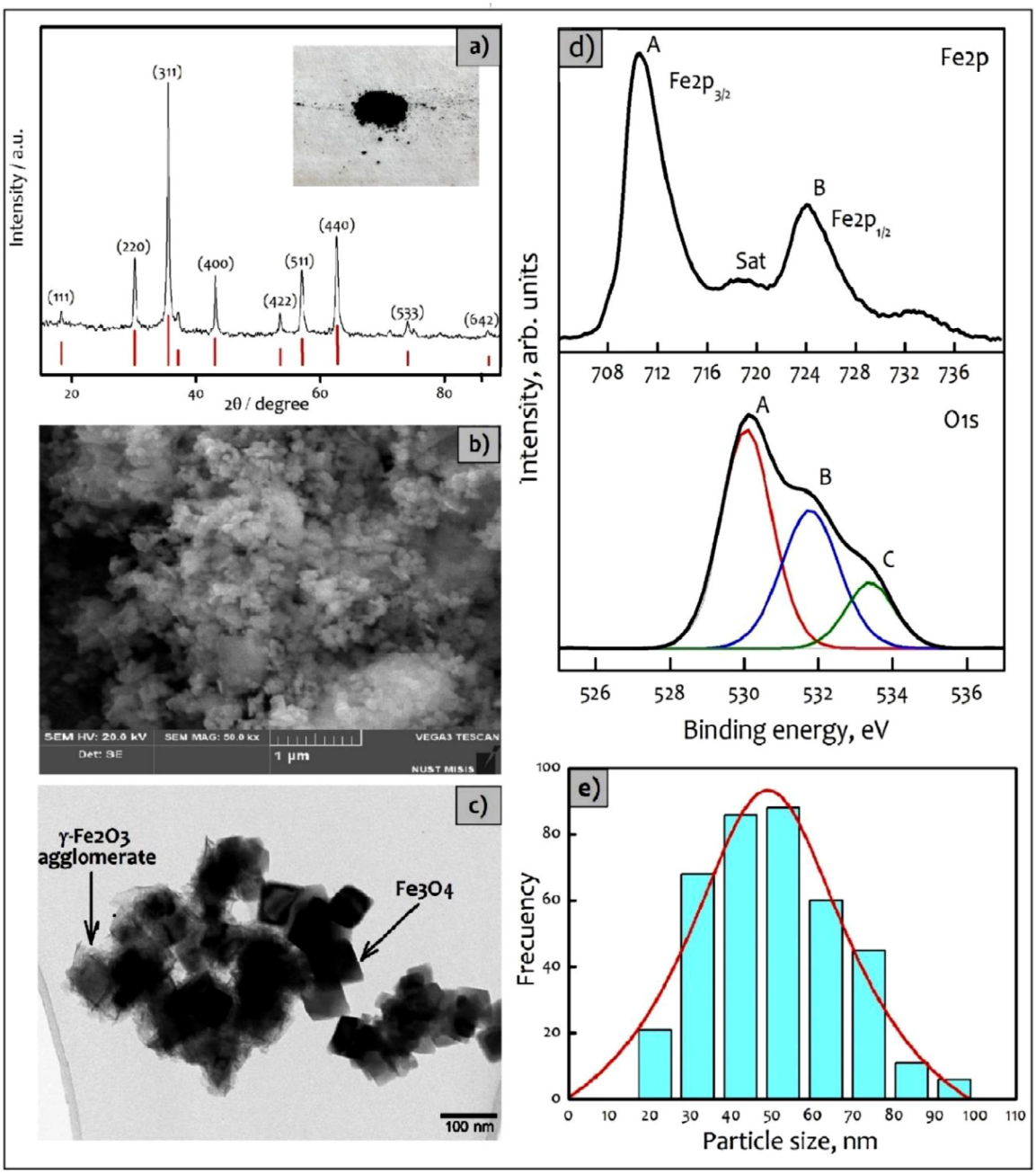

Fig. 1. a) XRD pattern, b) SEM and c) TEM images and e) particle size distribution of γ-Fe_2O_3/Fe_3O_4 nanocomposite; d) Fe2p (top) and O1s (bottom) spectra from the γ-Fe_2O_3/Fe_3O_4 nanocomposite's surface.

Fig. 1e demonstrates a histogram of the Fe_3O_4 particle size distribution obtained from TEM images. The results show that the Fe_3O_4 particle sizes range from 20 to 100 nm with an average grain size close to 50 nm. Thus, the particle size obtained by TEM is slightly higher than the crystallite size determined by XRD, that is consistent with data reported in the literature [41]. Fe_3O_4 nanoparticles tend to form clusters and short chains of octahedra along the (111) crystallographic direction due to inter-particle magnetic force [42].

The chemical state and surface composition of the γ-Fe_2O_3/Fe_3O_4 nanocomposite were analyzed by using XPS. The survey spectrum (Fig. S4) indicates the coexistence of Fe, O and C elements. The C1s line contains four components, which can be attributed to C–C, C–COO, CH_2–O and $C = O$ bonds and refers to hydrocarbon contamination of surface, since the nanocomposite powder was exposed to air before XPS studies [43].

The Fe2p and O1s spectra to make it possible to evaluate the chemical state of Fe on the nanocomposite's surface is shown in Fig. 1d. The O1s spectrum profile consists of three components A, B, and C with binding energies of 530.0 eV, 531.7 eV, and 533.3 eV, respectively, which are referred to Fe_2O_3 oxide, as well as oxygen chemisorbed on the nanocomposite surface and to oxygen of OH groups and water [44]. The Fe 2p spectrum shows the broad main peaks of Fe $2p_{3/2}$ and Fe $2p_{1/2}$ locate at 710.6 eV and 724.2 eV, respectively, which exhibit the typical structure of Fe_3O_4 nanoparticle in the composites [45]. However, the presence of a charge transfer satellite with an energy of 718.6 eV makes it possible to unambiguously assign the Fe chemical state on the nanocomposite surface to the bonds between O and Fe in Fe_2O_3 oxide, i.e. to ferric iron Fe^{3+} [46].

Moreover, the Fe3s spectrum was obtained to assess Fe magnetic state. As is known, the length between the high-spin and low-spin components in the Fe3s spectrum corresponds to the magnetic moment on the Fe atom [47]. The monocrystalline Fe_2O_3 magnetic moment leads to the Fe3s spectrum splitting up to 6.3 eV [48]. The obtained Fe3s spectrum splitting on the γ-Fe_2O_3/Fe_3O_4 nanocomposite surface is 6.8 eV. This indicates the presence existence of a larger local magnetic moment on the Fe atom located in the nanocomposite surface layer.

3.2. The study of the electrocatalytic activity of γ-Fe_2O_3/Fe_3O_4 nanocomposite

Hydrogen peroxide is reduced on a Fe_3O_4 cathode via the well-known mechanism as follows [19,49]:

$$2Fe^{3+} + H_2O_2 + \bar{e} \rightarrow HOO^{\cdot} + 2Fe^{2+} + H^+ \quad (1)$$

$$2Fe^{2+} + HOO^{\cdot} + H^+ \rightarrow 2Fe^{3+} + H_2O + \frac{1}{2}O_2 \quad (2)$$

The electrocatalytic activity of the γ-Fe_2O_3/Fe_3O_4 nanocomposite was studied using cyclic voltammetry (CV). Fig. 2a demonstrates the CV response of γ-Fe_2O_3/Fe_3O_4 sensor obtained in N_2-saturated 0.1 M KH_2PO_4 solution containing H_2O_2 with different concentrations. It can be seen that hydrogen peroxide reduction occurs at the potential nearly −250 mV. The rate of H_2O_2 reduction gradually increases with an increase in the hydrogen peroxide concentration that may be applied for quantitative analysis [19]. Meanwhile, the reduction current is drastically enhanced and the peaks of the $Fe^{2+}/^{3+}$ redox couple are disappeared, when H_2O_2 is added to the supporting electrolyte. This indicates an obvious electrocatalytic behavior of γ-Fe_2O_3/Fe_3O_4 nanocomposite during the reduction of H_2O_2 over a wide concentration range [18]. Fig. 2b shows the CV curves of the γ-Fe_2O_3/Fe_3O_4 nanocomposite recorded at different scan rates from 5 to 200 mV s^{-1}. It is obvious that the cathodic current increases with increasing the scan rate. Moreover, the relation between cathodic peak current at −300 mV and square root of sweep rate gives a straight line with a correlation coefficient of 0.9998 (inset in Fig. 2b) indicating that the redox process of the electrode surface is diffusion-controlled with an irreversible H_2O_2 electroreduction [18,19]. Besides, the electrochemically active surface area (ECSA) was also examined for evaluating the intrinsic activity of γ-Fe_2O_3/Fe_3O_4 nanocomposite. The roughness factor and the double-layer capacitance using the ΔI (I_a − I_c) versus the CVs scan rate (Fig. S5) were calculated to deduce ECSA. The electrochemical active surface area of γ-Fe_2O_3/Fe_3O_4 nanocomposite was estimated about 0.82 cm^2.

Various factors affecting the operation of the sensor were evaluated and the sensor was optimized to achieve maximum performance.

3.3. The influence of the Fe_3O_4 NPs amount and the supporting electrolyte optimization

A glassy carbon rotating disk electrode coated with different amount of γ-Fe_2O_3/Fe_3O_4 (1 - 12 mg mL^{-1}) was used to explore sensing performance of the prepared nanocomposite. As shown in Fig. 2c, the current response increases with an increase in amount of γ-Fe_2O_3/Fe_3O_4 to 7 mg mL^{-1} and decreases above 7 mg mL^{-1}. An appropriate amount of the γ-Fe_2O_3/Fe_3O_4 nanocomposite can improve the electron transfer. Further increase of the nanocomposite amount and the thickness of the film can lead to a decrease in the amperometric response due to hindering the electron transfer [4]. The optimal nanocomposite loading used in this work and was estimated to be 7 mg mL^{-1}. Furthermore, the charge transfer of γ-Fe_2O_3/Fe_3O_4 nanocomposite was evaluated by EIS measurements of different loading nanocomposite. As shown in Fig. S6, the Nyquist plots consist of two distinct parts: a linear part at low frequency and a semicircle part at high frequency for all nanocomposite loading. It is well known that a smaller arc radius means a smaller charge transfer resistance at the electrode/electrolyte interface [50,51]. The high-frequency semicircle starting from the Re (Ohm) axis negative region was apparently associated with the reference electrode behavior (its inertia) and no greater interest for analysis, since it is probably not related to the processes taking place on the working electrode. The low-frequency arc radius of the 7 mg mL^{-1} nanocomposite loading is smaller than with other loading, which indicates that the charge transfer layer resistance of the nanocomposite loading (7 mg mL^{-1}) interface was the smallest.

The pH value of 0.1 M KH_2PO_4 solution is very essential for the improvement of the electrocatalytic performance of the electrode modified with γ-Fe_2O_3/Fe_3O_4 nanocomposite [19].

Fig. 2d reveals the effect of pH varying from 7.0 to 7.6 on the amperometric response. As can be seen at pH values above 7.3, a noticeable decrease in the current response is observed. Therefore, the electrolytes with pH values in the range from 7,0 to 7,3 were selected for further testing.

3.4. The amperometric response of H_2O_2

It is worth noting that γ-Fe_2O_3/Fe_3O_4 sensor is very sensitive to the change of H_2O_2 concentration. Fig. 2e shows the typical amperometric responses of the γ-Fe_2O_3/Fe_3O_4 sensor upon the successive addition of H_2O_2 into the stirring (1000 rpm) 0.1 M KH_2PO_4 (pH = 7.3) solution. The operating potential was −300 mV. The current signal has a significant step and reaches a stable level within 2 s when a small amount of H_2O_2 is added. This short response time can be attributed to the fact that H_2O_2 is rapidly adsorbed on the surface of the γ-Fe_2O_3/Fe_3O_4 nanocomposite and its electroreduction process is activated [52].

The relationship between current and H_2O_2 concentration is presented in Fig. 2f. The γ-Fe_2O_3/Fe_3O_4 sensor shows two linear responses in the ranges of 200–1000 nM and > 100 μM (up to 8 mM tested in this work). The limit of detection around 50 nM can be obtained from this γ-Fe_2O_3/Fe_3O_4 nanocomposite based on a signal-to-noise ratio (S/N) of 3.

Table 1 shows the comparison of different electrodes for the H_2O_2 sensing ever reported. The proposed material displayed an excellent comprehensive performance and can be easily prepared by means of a fast and simple procedure. The γ-Fe_2O_3/Fe_3O_4 sensor has the lowest LOD compared with Fe_3O_4-based sensors and the wider linear range that may be due to the larger surface-area-to-volume ratio of magnetic iron oxide particles for H_2O_2 molecules to adsorb or react [53,54]. Therefore, the γ-Fe_2O_3/Fe_3O_4 nanocomposite prepared via an electrochemical method using pulse alternating current is an ideal electrode material for detecting H_2O_2.

Fig. 3(a–c) demonstrates the sensor response before and after washing and long-term stability of the γ-Fe_2O_3/Fe_3O_4 sensor. The γ-Fe_2O_3/Fe_3O_4 sensor has an excellent response to the sensing. There was no significant change in the amperometric response even after washing the sensor. These results indicate good stability γ-Fe_2O_3/Fe_3O_4 sensor towards the detection and determination of H_2O_2. Long-term stability of the developed sensor was evaluated by measuring its amperometric response towards 0.5 mM H_2O_2 over 8 days under room temperature. The sensor response remains quite stable with retention of about 83.4% after 8 days, showing good long-term stability of γ-Fe_2O_3/Fe_3O_4 at room temperature (Fig. 3c).

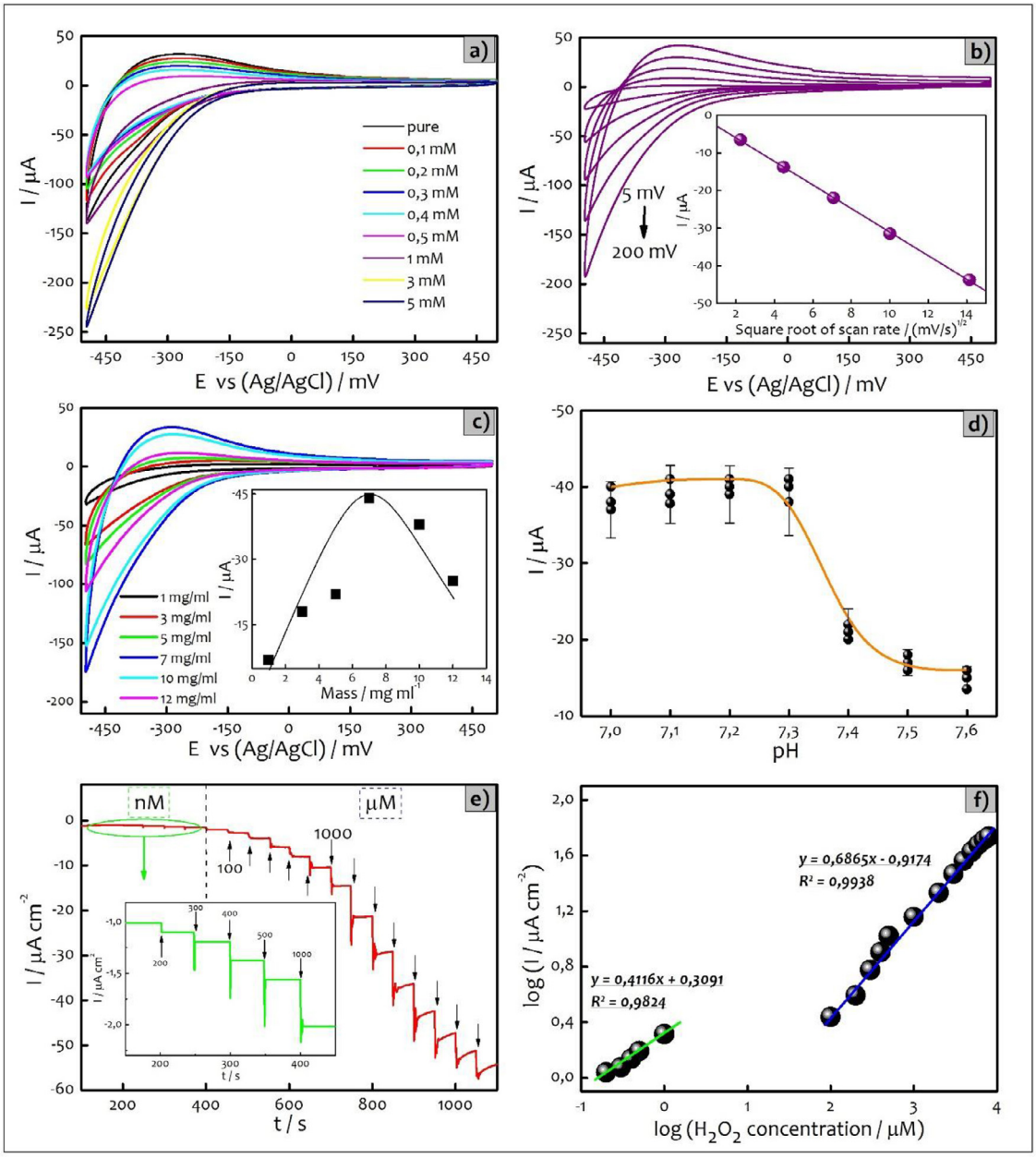

Fig. 2. The γ-Fe_2O_3/Fe_3O_4 sensor properties in N_2 saturated 0.1 M KH_2PO_4 (pH = 7.3) solution: a) CVs in the presence of different H_2O_2 concentrations at a scan rate of 100 mV s^{-1}: b) CVs at different scan rates in the presence of 1 mM H_2O_2 (Inset: linear relationship between the cathodic currents and the square root of scan rates); c) the influence of the γ-Fe_2O_3/Fe_3O_4 amount on H_2O_2 detection; d) the effect of the pH value on the amperometric responses of 1 mM H_2O_2; e) amperometric response with successive addition of H_2O_2 at potential of −300 mV (vs Ag/AgCl) into the stirring (1000 rpm) solution; f) the relationship between the amperometric response and the H_2O_2 concentration.

Table 1
The comparison of different electrodes for H_2O_2 detection.

Electrode	LOD (μM)	Linear range (mM)	Response time	Ref
Fe_3O_4	1000	–	–	[55]
Fe_3O_4–Fe_2O_3	200	0.2 - 1.8	<3s	[56]
Fe_3O_4/3DG NCs	0.078	–	<3s	[18]
3D - Fe_3O_4	2	0.005–4.995	–	[19]
Fe_3O_4@C–Cu/GCE	32.6	0.08 –372	–	[57]
AgNPs-P(ABA)-Fe_3O_4	1.74	0.005 - 5.5	–	[58]
SPCE|GS–Nafion/Fe_3O_4–Au-HRP	12	0.02–2.5	3s	[54]
γ-Fe_2O_3/Fe_3O_4	0.05	0.0002 - 8	2s	This work

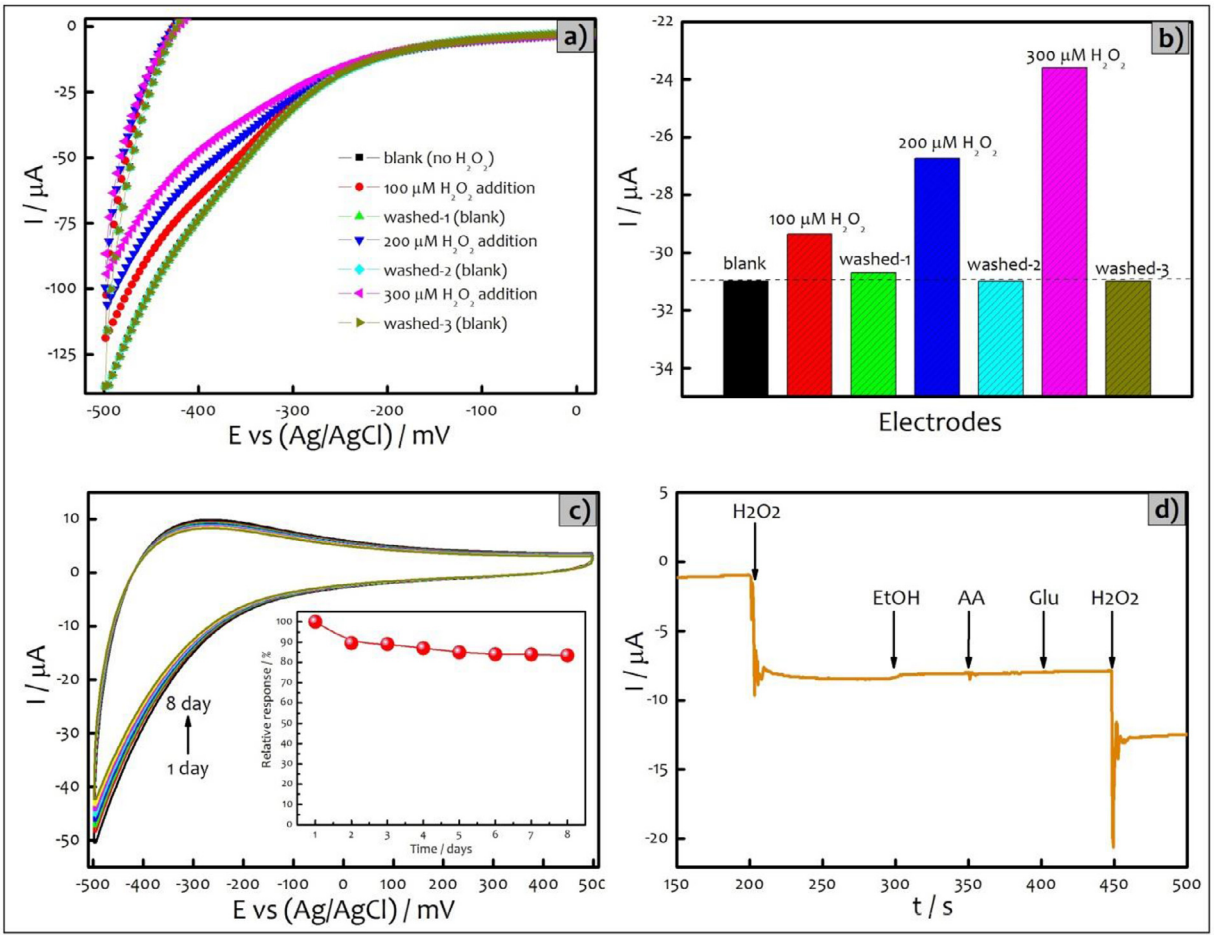

Fig. 3. (a–b) Stability of γ-Fe_2O_3/Fe_3O_4 sensor before and after washing towards H_2O_2 sensing at various additions; c) long-term stability of γ-Fe_2O_3/Fe_3O_4 sensor; d) an amperometric response of the γ-Fe_2O_3/Fe_3O_4 sensor to the successive addition of H_2O_2, EtOH, AA, Glu-and H_2O_2 (each 2 mM) respectively.

As it is well known, some co-existing physiological species including ethanol (EtOH), ascorbic acid (AA), and glucose (Glu), influence the sensor responses [57,58]. The amperometric responses of γ-Fe_2O_3/Fe_3O_4 to the consecutive addition of H_2O_2 (2 mM) and relevant electroactive species including EtOH, AA and Glu (each 2 mM) into the stirring (1000 rpm) 0.1 M KH_2PO_4 (pH = 7.3) solution were recorded (Fig. 3d). The γ-Fe_2O_3/Fe_3O_4 sensor was highly selective to H_2O_2 detection and displayed remarkable tolerance to interfering substances. These results indicate that our sensor exhibited good anti-interference ability in practical applications.

3.5. The formation mechanism of γ-Fe_2O_3/Fe_3O_4 nanocomposite via an electrochemical method using pulse alternating current

Electrochemical and chemical processes involving iron (ions, hydroxo-complexes, particles of oxides and hydroxides) are extremely diverse and complex. Various iron (III) hydroxo-compounds are formed in an aqueous medium mainly depending on the synthesis conditions [53,59]. There are 16 types of iron oxides and oxyhydroxides which occur comprising iron and oxygen [53].

We propose the following mechanism for γ-Fe_2O_3/Fe_3O_4 nanocomposite formation via an electrochemical PAC method taking into account the analysis of the oxidation products, the values of the electrode potentials in different synthesis periods and literature data [40,60–62]. The processes of water discharge with oxygen (3) and hydrogen (4) evolution during the anodic and cathodic pulses, respectively, are essential in determining a synthesis pathway. Electrochemical synthesis using PAC is characterized by the high-rate processes and intense gas bubbling under high current density in pulses.

$$4OH^- \rightarrow O_2 + 2H_2O + 4\bar{e} \quad (3)$$

$$2H_2O + 2\bar{e} \rightarrow 2OH^- + H_2 \quad (4)$$

Iron is oxidized during the anodic half-period (pulse and pause). In alkaline solutions, iron hydroxide (II) is formed via oxidation of iron (5) [63]:

$$Fe + 2H_2O \rightarrow Fe(OH)_2 + 2H^+ + 2\bar{e} \quad (5)$$

Moreover, $Fe(OH)_2$ can undergo a number of chemical (in solution or in solid phase) and electrochemical (on the electrode surface) transformations including oxygen-involved reactions (3). After a few minutes of the electrosynthesis the reaction media displayed a light brown color as a result of iron hydroxide (III) or ferric oxyhydroxide FeOOH (6) formation (Fig. 4a) [64]:

$$3Fe(OH)_2 + \frac{1}{2}O_2 \rightarrow Fe(OH)_2 + 2FeOOH + H_2O \quad (6)$$

Alternatively, a direct electrochemical generation of ferric oxyhydroxide involving iron oxidation process (7) is possible [65]:

$$Fe + 3OH^- \rightarrow \gamma - FeOOH + 3\bar{e} \quad (7)$$

The chemical interaction of ferric oxyhydroxide obtained by (6) and (7) and iron hydroxide (II) in solution is actual route of magnetite Fe_3O_4 formation (8) [64]:

$$Fe(OH)_2 + FeOOH \rightarrow Fe_3O_4 + 2H_2O \quad (8)$$

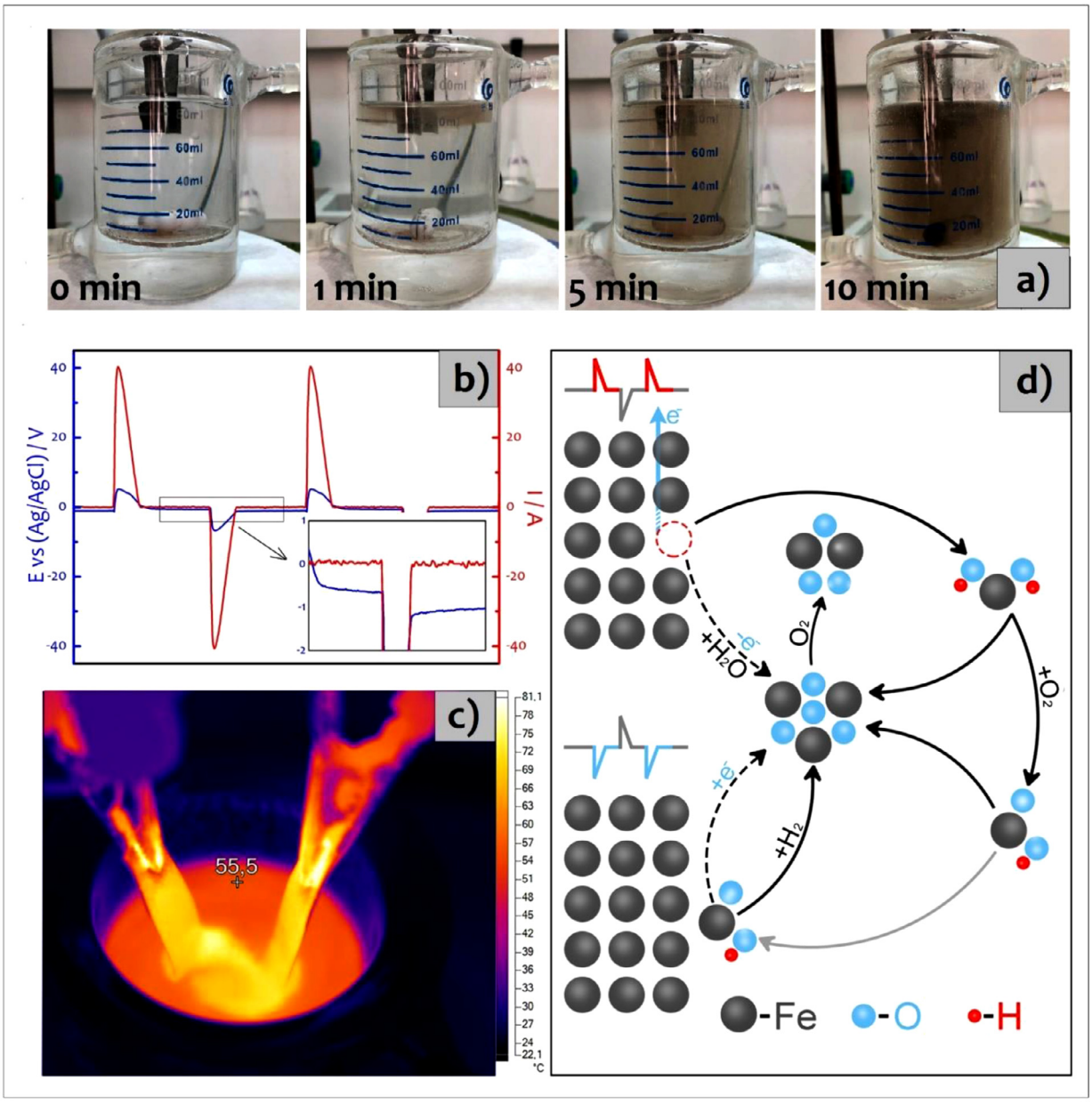

Fig. 4. a) The formation of γ-Fe_2O_3/Fe_3O_4 nanocomposite; b) electrode potential and current variation during synthesis; c) temperature gradient within electrochemical cell during synthesis. d) Scheme of the main chemical and electrochemical reactions of γ-Fe_2O_3/Fe_3O_4 nanocomposite formation involving iron under PAC in a NaOH solution.

The direct growth of magnetite on the electrode surface according to reaction (9) is plausible under severe pulsed electrosynthesis conditions [63]:

$$3Fe + 4H_2O \rightarrow Fe_3O_4 + 8H^+ + 8\bar{e} \quad (9)$$

Anodic water oxidation produces oxygen bubbles, which promote the removal of the already formed magnetite particles from the electrode surface. The suspended solids give a black color to indicate Fe_3O_4 formation (8, 9) (Fig. 4a).

An intense hydrogen bubbling (4) occurs via water reduction during the cathodic pulse and causes the electrode potential increase at the pulses due to ohmic losses (Fig. 4b) and electrolyte heating (Fig. 4c).

Additionally, ferric oxyhydroxide can be reduced to magnetite both electrochemically on the electrode surface (10) or chemically by generated hydrogen (11) [26]:

$$FeOOH + \bar{e} \rightarrow Fe_3O_4 + H_2O + OH^- \quad (10)$$

$$FeOOH + \frac{1}{2}H_2 \rightarrow Fe_3O_4 + 2H_2O \quad (11)$$

Magnetite Fe_3O_4 is thermodynamically unstable and rapidly converted to maghemite (isostructural to magnetite) even at room temperature [66]. The formation of a thin layer of maghemite γ-Fe_2O_3 proceeds via the diffusion of Fe^{2+}cations onto the nanoparticle surface and oxidation to Fe^{3+} in oxygen-saturated alkaline electrolyte under PAC synthesis conditions (12):

$$2Fe_3O_4 + \frac{1}{2}O_2 \rightarrow 3Fe_2O_3 \quad (12)$$

According to the above chemical and electrochemical reactions, the proposed scheme for the formation of Fe_2O_3/Fe_3O_4 nanocomposite under PAC in a NaOH solution is shown in Fig. 4d.

4. Conclusion

In summary, γ-Fe_2O_3/Fe_3O_4 nanocomposite was prepared via an electrochemical method using pulse alternating current and was characterized by XRD, TG/DSC, XPS, SEM and TEM. The mechanism of γ-Fe_2O_3/Fe_3O_4 nanocomposite formation was proposed. The sensor exhibited a fast electron transfer process in γ-Fe_2O_3/Fe_3O_4 nanocomposite. The optimized H_2O_2 sensor revealed a remarkable low limit of detection of 0.05 μM, a wide linear range from 0.0002 to 8 mM, and a fast response time of 2 s. These results demonstrated that γ-Fe_2O_3/Fe_3O_4 prepared via an electrochemical method using pulse alternating current is a promising efficient material for electrochemical sensing of H_2O_2.

Declaration of Competing Interest

The authors declare that they have no known competing financial interests or personal relationships that could have appeared to influence the work reported in this paper.

Funding

The authors thank the Shared Research Center “Nanotechnologies” of Platov South-Russian State Polytechnic University (NPI) for XRD analyses. The research was financially supported by Russian Science Foundation (project № 20-79-10063).

Supplementary materials

Supplementary material associated with this article can be found, in the online version, at doi:10.1016/j.electacta.2020.137723.

References

[1] R. Ramachandran, C. Zhao, M. Rajkumar, K. Rajavel, P. Zhu, W. Xuan, Z.-.X. Xu, F. Wang, Porous nickel oxide microsphere and $Ti_3C_2T_x$ hybrid derived from metal-organic framework for battery-type supercapacitor electrode and non-enzymatic H_2O_2 sensor, Electrochim. Acta 322 (2019) 134771, doi:10.1016/j.electacta.2019.134771.

[2] L. Ning, X. Guan, J. Ma, M. Wang, X. Fan, G. Zhang, F. Zhang, W. Peng, Y. Li, A highly sensitive nonenzymatic H_2O_2 sensor based on platinum, $ZnFe_2O_4$ functionalized reduced graphene oxide, J. Alloys Compd. 738 (2018) 317–322, doi:10.1016/j.jallcom.2017.12.161.

[3] J. Meier, E.M. Hofferber, J.A. Stapleton, N.M. Iverson, Hydrogen peroxide sensors for biomedical applications, Chemosensors 7 (2019), doi:10.3390/chemosensors7040064.

[4] L. Cai, B. Hou, Y. Shang, L. Xu, B. Zhou, X. Jiang, X. Jiang, Synthesis of Fe_3O_4/graphene oxide/pristine graphene ternary composite and fabrication electrochemical sensor to detect dopamine and hydrogen peroxide, Chem. Phys. Lett. 736 (2019) 136797, doi:10.1016/j.cplett.2019.136797.

[5] G. Pizzino, N. Irrera, M. Cucinotta, G. Pallio, F. Mannino, V. Arcoraci, F. Squadrito, D. Altavilla, A. Bitto, Oxidative stress: harms and benefits for human health, Oxid. Med. Cell. Longev. 2017 (2017) 8416763, doi:10.1155/2017/8416763.

[6] S. Majumder, B. Saha, S. Dey, R. Mondal, S. Kumar, S. Banerjee, A highly sensitive non-enzymatic hydrogen peroxide and hydrazine electrochemical sensor based on 3D micro-snowflake architectures of α-Fe_2O_3, RSC Adv. 6 (2016) 59907–59918, doi:10.1039/C6RA10470C.

[7] A. Koyappayil, S. Berchmans, M.-.H. Lee, Dual enzyme-like properties of silver nanoparticles decorated Ag_2WO_4 nanorods and its application for H_2O_2 and glucose sensing, Colloids Surf. B Biointerfaces 189 (2020) 110840, doi:10.1016/j.colsurfb.2020.110840.

[8] H. Chen, A. Fang, L. He, Y. Zhang, S. Yao, Sensitive fluorescent detection of H_2O_2 and glucose in human serum based on inner filter effect of squaric acid-iron(III) on the fluorescence of upconversion nanoparticle, Talanta 164 (2017) 580–587, doi:10.1016/j.talanta.2016.10.008.

[9] C. Zhao, H. Cui, J. Duan, S. Zhang, J. Lv, Self-catalyzing chemiluminescence of luminol-diazonium ion and its application for catalyst-free hydrogen peroxide detection and rat arthritis imaging, Anal. Chem. 90 (2018) 2201–2209, doi:10.1021/acs.analchem.7b04544.

[10] H. Zhang, J. Ruan, W. Liu, X. Jiang, T. Du, H. Jiang, P. Alberto, K.-.E. Gottschalk, X. Wang, Monitoring dynamic release of intracellular hydrogen peroxide through a microelectrode based enzymatic biosensor, Anal. Bioanal. Chem. 410 (2018) 4509–4517, doi:10.1007/s00216-018-1108-5.

[11] A. Sukeri, A.S. Lima, M. Bertotti, Development of non-enzymatic and highly selective hydrogen peroxide sensor based on nanoporous gold prepared by a simple unusual electrochemical approach, Microchem. J. 133 (2017) 149–154, doi:10.1016/j.microc.2017.03.023.

[12] D. Yin, X. Bo, J. Liu, L. Guo, A novel enzyme-free glucose and H_2O_2 sensor based on 3D graphene aerogels decorated with Ni_3N nanoparticles, Anal. Chim. Acta 1038 (2018) 11–20, doi:10.1016/j.aca.2018.06.086.

[13] N.H. Al-Hardan, M.A. Abdul Hamid, R. Shamsudin, E.M. Al-Khalqi, L. Kar Keng, N.M. Ahmed, Electrochemical hydrogen peroxide sensor based on macroporous silicon, Sens. Basel 18 (2018) 716, doi:10.3390/s18030716.

[14] H. Shamkhalichenar, J.-.W. Choi, Review—non-enzymatic hydrogen peroxide electrochemical sensors based on reduced graphene oxide, J. Electrochem. Soc. 167 (2020) 37531, doi:10.1149/1945-7111/ab644a.

[15] K. Dhara, D. Mahapatra, Recent advances in electrochemical nonenzymatic hydrogen peroxide sensors based on nanomaterials: a review, J. Mater. Sci. (2019) 54, doi:10.1007/s10853-019-03750-y.

[16] R. Suhanto, R. Rahmawati, D. Setyorini, I. Noviandri, S. Suyatman, B. Yuliarto, Modified working electrode by magnetite nanocomposite for electrochemical sensor application, IOP Conf. Ser. Mater. Sci. Eng. 367 (2018) 12054, doi:10.1088/1757-899X/367/1/012054.

[17] P. Tipsawat, U. Wongpratat, S. Phumying, N. Chanlek, K. Chokprasombat, S. Maensiri, Magnetite (Fe_3O_4) nanoparticles: synthesis, characterization and electrochemical properties, Appl. Surf. Sci. 446 (2018) 287–292, doi:10.1016/j.apsusc.2017.11.053.

[18] Y. Zhao, D. Huo, J. Bao, M. Yang, M. Chen, J. Hou, H. Fa, C. Hou, Biosensor based on 3D graphene-supported Fe_3O_4 quantum dots as biomimetic enzyme for in situ detection of H_2O_2 released from living cells, Sens. Actuators B Chem. 244 (2017) 1037–1044, doi:10.1016/j.snb.2017.01.029.

[19] K. Yang, H. Zhong, Z. Cheng, X. Li, A. Zhang, T. Li, Y. Zhang, G. Liu, H. Qian, Magnetic Fe_3O_4 stacked sphere-like nanocomposite and its application as platform for H_2O_2 sensing, J. Electroanal. Chem. 814 (2018) 1–6, doi:10.1016/j.jelechem.2018.02.040.

[20] F. Moreira, E.R. Santana, A. Spinelli, Ionic liquid-supported magnetite nanoparticles as electrode modifier materials for estrogens sensing, Sci. Rep. 10 (2020) 1955, doi:10.1038/s41598-020-58931-6.

[21] P. Herrasti, E. Mazarío, F.J. Recio, Improved magnetosensor for the detection of hydrogen peroxide and glucose, J. Solid State Electrochem. (2020), doi:10.1007/s10008-020-04649-4.

[22] S. Majidi, F. Sehrig, S. mussa farkhani, M. Soleymani-Goloujeh, A. Akbarzadeh, Current methods for synthesis of magnetic nanoparticles, Artif. Cells Nanomed. Biotechnol. 44 (2014) 1–13, doi:10.3109/21691401.2014.982802.

[23] M. Aliahmad, N. Moghaddam, Synthesis of maghemite (γ-Fe_2O_3) nanoparticles by thermal-decomposition of magnetite (Fe_3O_4) nanoparticles, Mater. Sci. (2013) 31, doi:10.2478/s13536-012-0100-6.

[24] Q. Zhao, J. Liu, Y. Wang, W. Tian, J. Liu, J. Zang, H. Ning, C. Yang, M. Wu, Novel in-situ redox synthesis of Fe_3O_4/rGO composites with superior electrochemical performance for lithium-ion batteries, Electrochim. Acta 262 (2018) 233–240, doi:10.1016/j.electacta.2018.01.019.

[25] N. Rezaei, M.H. Ehsani, M. Aghazadeh, I. Karimzadeh, An investigation on magnetic-interacting Fe_3O_4 nanoparticles prepared by electrochemical synthesis method, J. Supercond. Nov. Magn. 31 (2018) 2139–2147, doi:10.1007/s10948-017-4445-2.

[26] A. Rodriguez, A. Paredes-Arroyo, J. Mojica-Gomez, C. Estrada-Arteaga, J. Cruz-Rivera, C. Elias, R. Antaño-López, Electrochemical synthesis of magnetite and maghemite nanoparticles using dissymmetric potential pulses, J. Nanoparticle Res. (2012) 14, doi:10.1007/s11051-012-0993-3.

[27] A. Ulyankina, M. Avramenko, D. Kusnetsov, K. Firestein, D. Zhigunov, N. Smirnova, Electrochemical synthesis of TiO_2 under pulse alternating current: effect of thermal treatment on the photocatalytic activity, Chem. Select 4 (2019) 2001–2007, doi:10.1002/slct.201803367.

[28] D. Chernysheva, C. Vlaic, I. Leontyev, L. Pudova, S. Ivanov, M. Avramenko, M. Allix, A. Rakhmatullin, O. Maslova, A. Bund, N. Smirnova, Synthesis of Co_3O_4/CoOOH via electrochemical dispersion using a pulse alternating current method for lithium-ion batteries and supercapacitors, Solid State Sci. 86 (2018) 53–59, doi:10.1016/j.solidstatesciences.2018.10.005.

[29] A. Ulyankina, I. Leontyev, O. Maslova, M. Allix, A. Rakhmatullin, N. Nevzorova, R. Valeev, G. Yalovega, N. Smirnova, Copper oxides for energy storage application: novel pulse alternating current synthesis, Mater. Sci. Semicond. Process. 73 (2018) 111–116, doi:10.1016/j.mssp.2017.08.001.

[30] A.A. Ulyankina, A.B. Kuriganova, N.V. Smirnova, Photocatalytic properties of SnO_2–SnO nanocomposite prepared via pulse alternating current synthesis, Mendeleev Commun. 29 (2019) 215–217, doi:10.1016/j.mencom.2019.03.034.

[31] D.V. Leontyeva, I.N. Leontyev, M.V. Avramenko, Y.I. Yuzyuk, Y.A. Kukushkina, N.V. Smirnova, Electrochemical dispergation as a simple and effective technique toward preparation of NiO based nanocomposite for supercapacitor application, Electrochim. Acta 114 (2013) 356–362, doi:10.1016/j.electacta.2013.10.031.

[32] K. Ye, Z. Zhou, J. Shao, L. Lin, D. Gao, N. Ta, R. Si, G. Wang, X. Bao, In situ reconstruction of a hierarchical Sn-Cu/SnO_x core/shell catalyst for high-performance CO_2 electroreduction, Angew. Chem. Int. Ed. 59 (2020) 4814–4821, doi:10.1002/anie.201916538.

[33] K. Ye, A. Cao, J. Shao, G. Wang, R. Si, N. Ta, J. Xiao, G. Wang, Synergy effects on Sn-Cu alloy catalyst for efficient CO_2 electroreduction to formate with high mass activity, Sci. Bull. 65 (2020) 711–719, doi:10.1016/j.scib.2020.01.020.

[34] Y.H. Chen, Thermal properties of nanocrystalline goethite, magnetite, and maghemite, J. Alloys Compd. 553 (2013) 194–198, doi:10.1016/j.jallcom.2012.11.102.
[35] V.N. Nikiforov, A.N. Ignatenko, V.Y. Irkhin, Size and surface effects on the magnetism of magnetite and maghemite nanoparticles, J. Exp. Theor. Phys. 124 (2017) 304–310, doi:10.1134/S1063776117010046.
[36] J.P. Sanders, P.K. Gallagher, Kinetics of the oxidation of magnetite using simultaneous TG/DSC, J. Therm. Anal. Calorim. 72 (2003) 777–789, doi:10.1023/A:1025053828639.
[37] M. Ounacer, A. Essoumhi, M. Sajieddine, A. Razouk, B.F.O. Costa, S.M. Dubiel, M. Sahlaoui, Structural and magnetic studies of annealed iron oxide nanoparticles, J. Supercond. Nov. Magn. 33 (2020) 3249–3261, doi:10.1007/s10948-020-05586-z.
[38] T. Costa, E. Baldi, A. Figueiró, G. Lopes Colpani, L. Silva, M. Zanetti, J. Mello, M. Fiori, Fe_3O_4@C core-shell nanoparticles as adsorbent of ionic zinc: evaluating of the adsorptive capacity, Mater. Res. (2019) 22, doi:10.1590/1980-5373-mr-2018-0847.
[39] P.T.L. Huong, L.T. Huy, H. Lan, L.H. Thang, T.T. An, N. Van Quy, P.A. Tuan, J. Alonso, M.-.H. Phan, A.-.T. Le, Magnetic iron oxide-carbon nanocomposites: impacts of carbon coating on the As(V) adsorption and inductive heating responses, J. Alloys Compd. 739 (2018) 139–148, doi:10.1016/j.jallcom.2017.12.178.
[40] S. Kronmuller, H., Waser, R., Bottger, U., Tiedke, Handbook of magnetism and advanced magnetic materials, 2007.
[41] S. Schwaminger, S.P. Bauer, D. Fraga-García, P. Wagner, F.E. Berensmeier, Oxidation of magnetite nanoparticles: impact on surface and crystal properties, CrystEngComm 19 (2017) 246–255.
[42] R. Rahmawati, A. Taufiq, B.Y. Sunaryono, Nugraha Suyatman, I. Noviandri, D.A. Setyorini, D. Kurniadi, The synthesis of Fe_3O_4/MWCNT nanocomposites from local iron sands for electrochemical sensors, AIP Conf. Proc. 1958 (2018) 20016, doi:10.1063/1.5034547.
[43] B. Lesiak, N. Rangam, P. Jiricek, I. Gordeev, J. Tóth, L. Kövér, M. Mohai, P. Borowicz, Surface study of Fe_3O_4 nanoparticles functionalized with biocompatible adsorbed molecules, Front. Chem. 7 (2019) 642, doi:10.3389/fchem.2019.00642.
[44] X. Wang, Y. Liu, H. Arandiyan, H. Yang, L. Bai, J. Mujtaba, Q. Wang, S. Liu, H. Sun, Uniform Fe_3O_4 microflowers hierarchical structures assembled with porous nanoplates as superior anode materials for lithium-ion batteries, Appl. Surf. Sci. 389 (2016) 240–246, doi:10.1016/j.apsusc.2016.07.105.
[45] X. Qian Tang, Y. Dan Zhang, Z. Wei Jiang, D. Mei Wang, C. Zhi Huang, Y. Fang Li, Fe_3O_4 and metal–organic framework MIL-101(Fe) composites catalyze luminol chemiluminescence for sensitively sensing hydrogen peroxide and glucose, Talanta 179 (2018) 43–50, doi:10.1016/j.talanta.2017.10.049.
[46] T. Yamashita, P. Hayes, Analysis of XPS spectra of Fe^{2+} and Fe^{3+} ions in oxide materials, Appl. Surf. Sci. 254 (2008) 2441–2449, doi:10.1016/j.apsusc.2007.09.063.
[47] J.F. van Acker, Z.M. Stadnik, J.C. Fuggle, H.J.W.M. Hoekstra, K.H.J. Buschow, G. Stroink, Magnetic moments and x-ray photoelectron spectroscopy splittings in Fe3s core levels of materials containing Fe, Phys. Rev. B 37 (1988) 6827–6834, doi:10.1103/PhysRevB.37.6827.
[48] A.T. Kozakov, A.G. Kochur, K.A. Googlev, A.V. Nikolsky, I.P. Raevski, V.G. Smotrakov, V.V. Yeremkin, X-ray photoelectron study of the valence state of iron in iron-containing single-crystal ($BiFeO_3$, $PbFe_{1/2}Nb_{1/2}O_3$), and ceramic ($BaFe_{1/2}Nb_{1/2}O_3$) multiferroics, J. Electron Spectros. Relat. Phenom. 184 (2011) 16–23, doi:10.1016/j.elspec.2010.10.004.
[49] Y. Wang, H. Zhong, X. Li, X. Zhang, Z. Cheng, Z. Zhang, Y. Zhang, P. Chen, L. Zhang, L. Ding, J. Wang, Electrochemical temperature-controlled switch for nonenzymatic biosensor based on Fe_3O_4-PNIPAM microgels, J. Electroanal. Chem. 851 (2019) 113410, doi:10.1016/j.jelechem.2019.113410.
[50] S. Chen, H. Liang, M. Shen, Y. Jin, Yolk-like Fe_3O_4@C–Au@void@TiO_2–Pd hierarchical microspheres with visible light-assisted enhanced photocatalytic degradation of dye, Appl. Phys. A (2018) 124, doi:10.1007/s00339-018-1724-0.
[51] X. Chen, X. Liu, X. Yang, Y. Yang, A ternary magnetic recyclable ZnO/Fe_3O_4/g-C_3N_4 composite photocatalyst for efficient photodegradation of monoazo dye, Nanoscale Res. Lett. 14 (2019), doi:10.1186/s11671-019-2974-2.
[52] X. Sun, S. Guo, Y. Liu, S. Sun, Dumbbell-like PtPd– Fe_3O_4 nanoparticles for enhanced electrochemical detection of H_2O_2, Nano Lett. 12 (2012) 4859–4863, doi:10.1021/nl302358e.
[53] A. Ali, H. Zafar, M. Zia, I. Ul Haq, A.R. Phull, J.S. Ali, A. Hussain, Synthesis, characterization, applications, and challenges of iron oxide nanoparticles, Nanotechnol. Sci. Appl. 9 (2016) 49–67, doi:10.2147/NSA.S99986.
[54] Y. Xin, X. Fu-bing, L. Hong-wei, W. Feng, C. Di-zhao, W. Zhao-yang, A novel H_2O_2 biosensor based on Fe_3O_4–Au magnetic nanoparticles coated horseradish peroxidase and graphene sheets–Nafion film modified screen-printed carbon electrode, Electrochim. Acta 109 (2013) 750–755, doi:10.1016/j.electacta.2013.08.011.
[55] G. Cao, P. Wang, X. Li, Y. Wang, G. Wang, J. Li, Hydrogen peroxide electrochemical sensor based on Fe_3O_4 nanoparticles, Micro Nano Lett. IET 9 (2014) 16–18, doi:10.1049/mnl.2013.0612.
[56] G. Cao, P. Wang, X. Li, Y. Wang, G. Wang, J. Li, A sensitive nonenzymatic hydrogen peroxide sensor based on Fe_3O_4–Fe_2O_3 nanocomposites, Bull. Mater. Sci. (2015) 38, doi:10.1007/s12034-014-0803-x.
[57] M. Zhang, Q. Sheng, F. Nie, J. Zheng, Synthesis of Cu nanoparticles-loaded Fe_3O_4@carbon core–shell nanocomposite and its application for electrochemical sensing of hydrogen peroxide, J. Electroanal. Chem. 730 (2014) 10–15, doi:10.1016/j.jelechem.2014.07.020.
[58] M. Amatatongchai, S. Chairam, W. Sroysee, C. Boonchit, C. Kaewprom, T. Wangnoi, P. Jarujamrus, S. Tamaung, E. Somsook, Nonenzymatic sensor for hydrogen peroxide using a carbon paste electrode modified with a composite consisting of silver nanoparticles, poly(o-aminobenzoic acid) and magnetite, Int. J. Electrochem. Sci. 10 (2015) 4611–4625.
[59] F.N. Sayed, V. Polshettiwar, Facile and sustainable synthesis of shaped iron oxide nanoparticles: effect of iron precursor salts on the shapes of iron oxides, Sci. Rep. 5 (2015) 9733, doi:10.1038/srep09733.
[60] G. Parkinson, Iron oxide surfaces, Surf. Sci. Rep. (2016), doi:10.1016/j.surfrep.2016.02.001.
[61] R.M. Cornell, U. Schwertmann, The iron oxides: structure, properties, reactions, occurences and uses, Second Edition, 2003. 10.1002/3527602097.
[62] M. Pourbaix, Atlas of electrochemical equilibria in aqueous solutions, (1974). http://books.google.com/books?id=QjxRAAAAMAAJ.
[63] M. Popczyk, B. Losiewicz, The hydrogen evolution reaction on Fe electrode material in 1M NaOH solution, Solid State Phenom. 228 (2015) 252–257, doi:10.4028/www.scientific.net/SSP.228.252.
[64] F. Fajaroh, Y. Nazriati, S. Marfu'ah, A.N. Sumari, Synthesis of Fe_3O_4 nanoparticles using PEG template by electrochemical method, J. Phys. Conf. Ser. 1093 (2018) 12022, doi:10.1088/1742-6596/1093/1/012022.
[65] S. Franger, P. Berthet, J. Berthon, Electrochemical synthesis of Fe_3O_4 nanoparticles in alkaline aqueous solutions containing complexing agents, J. Solid State Electrochem. 8 (2004) 218–223, doi:10.1007/s10008-003-0469-6.
[66] S. Ramimoghadam, D. Bagheri, S. Hamid, Progress in electrochemical synthesis of magnetic iron oxide nanoparticles, J. Magn. Magn. Mater. 368 (2014) 207–229.